

**Figure S1: Basic assumptions of Mendelian randomisation.** (1) Relevance – genetic data, denoted by  $G$ , is robustly associated with the exposure. (2) Exchangeability –  $G$  is not associated with any confounder of the exposure-outcome relationship. (3) Exclusion restriction –  $G$  is independent of the outcome conditional on the exposure and all confounders of the exposure-outcome relationship (i.e. the only path between the instrument and the outcome is via the exposure).

1009 **1.1 Likelihood function identifiability**

1010 The likelihood function is symmetric around  $U$ , but for simplicity we will consider the general  
 1011 case where the variables of  $U$  and  $X$  are flipped, although the same can be said for the variables  
 1012 of  $U$  and  $Y$ . The likelihood function is partially identifiable such that there exists for any given  
 1013 model parameters, another model with different parameters but with the exact same likelihood  
 1014 function.

1015 Proof: given that the SNPs effects between trait  $X$  and the confounder  $U$  are flipped, the new  
 1016 parameters follow the following structure:

$$\begin{aligned}
 h'_x &= t_x + t_y \cdot \alpha_{y \rightarrow x} \\
 h'_y &= h_y \\
 \alpha'_{y \rightarrow x} &= \alpha_{y \rightarrow x} \\
 \alpha'_{x \rightarrow y} &= \frac{q_x \cdot \alpha_{x \rightarrow y} + q_y}{q_x + q_y \cdot \alpha_{y \rightarrow x}} \\
 &= \frac{q_x(\alpha_{x \rightarrow y} + \frac{q_y}{q_x})}{q_x(1 + \frac{q_y}{q_x} \cdot \alpha_{y \rightarrow x})} \\
 &= \frac{\alpha_{x \rightarrow y} + \frac{q_y}{q_x}}{1 + \frac{q_y}{q_x} \cdot \alpha_{y \rightarrow x}}
 \end{aligned}$$

1017 through inverse transformation,

$$\alpha_{x \rightarrow y} = \frac{\alpha'_{x \rightarrow y} + \frac{q'_y}{q'_x}}{1 + \frac{q'_y}{q'_x} \cdot \alpha_{y \rightarrow x}}$$

1018 Plugging in  $\alpha'_{x \rightarrow y}$  in the above equation, and simplifying  $\frac{ty}{tx}$  by  $w$  and  $\frac{ty'}{tx'}$  by  $w'$  to get the  
 1019 confounding ratio:

$$\begin{aligned}
 \alpha_{x \rightarrow y} &= \frac{\alpha'_{x \rightarrow y} + w'}{1 + w' \cdot \alpha_{y \rightarrow x}} \\
 \alpha_{x \rightarrow y} + \alpha_{x \rightarrow y} \cdot w' \cdot \alpha_{y \rightarrow x} &= \alpha'_{x \rightarrow y} + w' \\
 \alpha_{x \rightarrow y} - \alpha'_{x \rightarrow y} &= w' - \alpha_{x \rightarrow y} \cdot w' \cdot \alpha_{y \rightarrow x} \\
 \alpha_{x \rightarrow y} - \alpha'_{x \rightarrow y} &= w'(1 - \alpha_{x \rightarrow y} \cdot \alpha_{y \rightarrow x}) \\
 w' &= \frac{\alpha_{x \rightarrow y} - \alpha'_{x \rightarrow y}}{1 - \alpha_{x \rightarrow y} \cdot \alpha_{y \rightarrow x}}
 \end{aligned}$$

1020 inserting the complete form of  $\alpha'_{x \rightarrow y}$ ,

$$\begin{aligned}
w' &= \frac{\alpha_{x \rightarrow y} - \frac{\alpha_{x \rightarrow y} + \frac{q_y}{q_x}}{1 + \frac{q_y}{q_x} \alpha_{y \rightarrow x}}}{1 - \alpha_{x \rightarrow y} \cdot \alpha_{y \rightarrow x}} \\
&= \frac{\alpha_{x \rightarrow y} (1 + w \cdot \alpha_{y \rightarrow x}) - w - \alpha_{x \rightarrow y}}{(1 - \alpha_{x \rightarrow y} \cdot \alpha_{y \rightarrow x})(1 + w \cdot \alpha_{y \rightarrow x})} \\
&= \frac{\alpha_{x \rightarrow y} \cdot w \cdot \alpha_{y \rightarrow x} - w}{(1 - \alpha_{x \rightarrow y} \cdot \alpha_{y \rightarrow x})(1 + w \cdot \alpha_{y \rightarrow x})} \\
&= \frac{w(\alpha_{x \rightarrow y} \cdot \alpha_{y \rightarrow x} - 1)}{(1 - \alpha_{x \rightarrow y} \cdot \alpha_{y \rightarrow x})(1 + w \cdot \alpha_{y \rightarrow x})} \\
&= \frac{-w}{1 + w \cdot \alpha_{y \rightarrow x}}
\end{aligned}$$

1021 In order to obtain  $t'_y$  and  $t'_x$ , we use the equations of  $h'_x$ ,  $\alpha'_{x \rightarrow y}$  and by using the inverse trans-  
1022 formation of  $\alpha'_{y \rightarrow x} = \alpha_{y \rightarrow x}$ ,  $\alpha_{x \rightarrow y}$  as well as  $w'$  as follows:

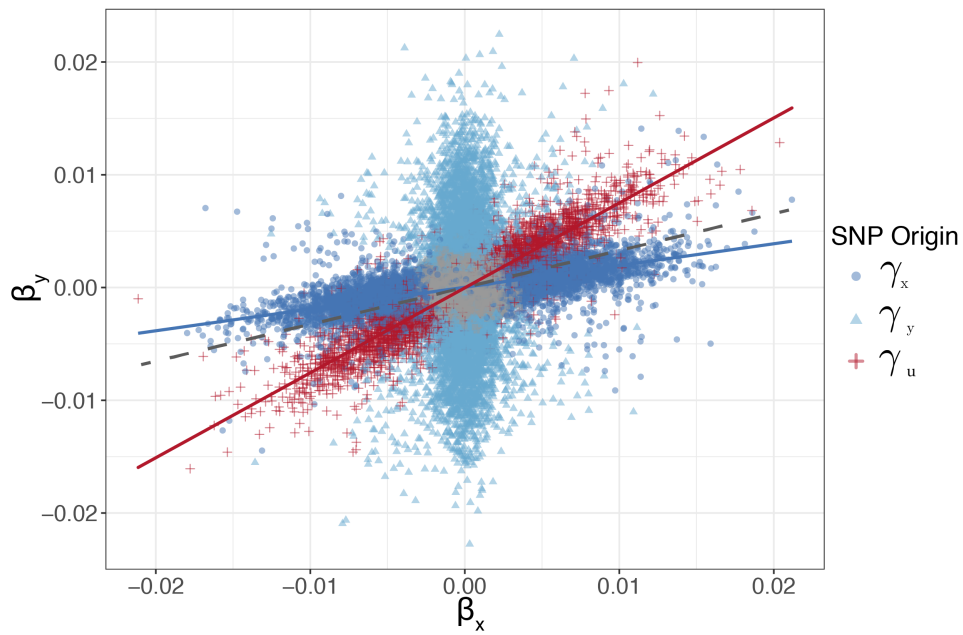
$$\begin{aligned}
t'_y &= \frac{-t'_x \cdot w}{1 + w \cdot \alpha_{y \rightarrow x}} \\
h_x &= t'_x + t'_y \cdot \alpha_{y \rightarrow x} \\
&= t'_x + \frac{-t'_x \cdot w}{1 + w \cdot \alpha_{y \rightarrow x}} \cdot \alpha_{y \rightarrow x} \\
&= \frac{t'_x + t'_x \cdot w \cdot \alpha_{y \rightarrow x} - t'_x \cdot w \cdot \alpha_{y \rightarrow x}}{1 + w \cdot \alpha_{y \rightarrow x}} \\
&= \frac{t'_x}{1 + w \cdot \alpha_{y \rightarrow x}} \\
t'_x &= h_x (1 + w \cdot \alpha_{y \rightarrow x})
\end{aligned}$$

1023 Replacing  $t'_x$  in  $h_x$  to get  $t'_y$ :

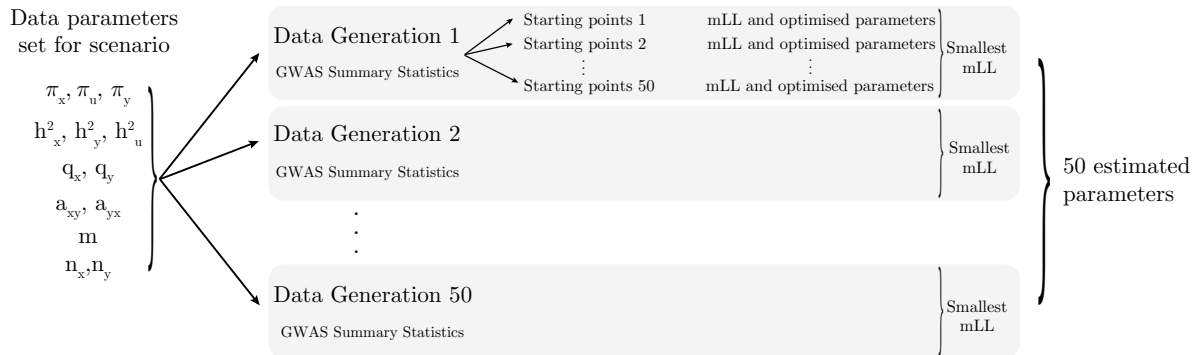
$$t'_y = h_x \cdot w$$

1024 Under these two models with equal likelihood, there are three slopes obtained from the ob-  
1025 served data: two are the correlation of effect sizes ( $\alpha_{x \rightarrow y}$  and  $1/\alpha_{y \rightarrow x}$ ), where one of them is  
1026 greater than, and the other is within the parameter bounds. The third is the correlation of the  
1027 confounder  $\frac{\alpha_{x \rightarrow y} + \frac{q_y}{q_x}}{1 + \frac{q_y}{q_x} \alpha_{y \rightarrow x}}$ .

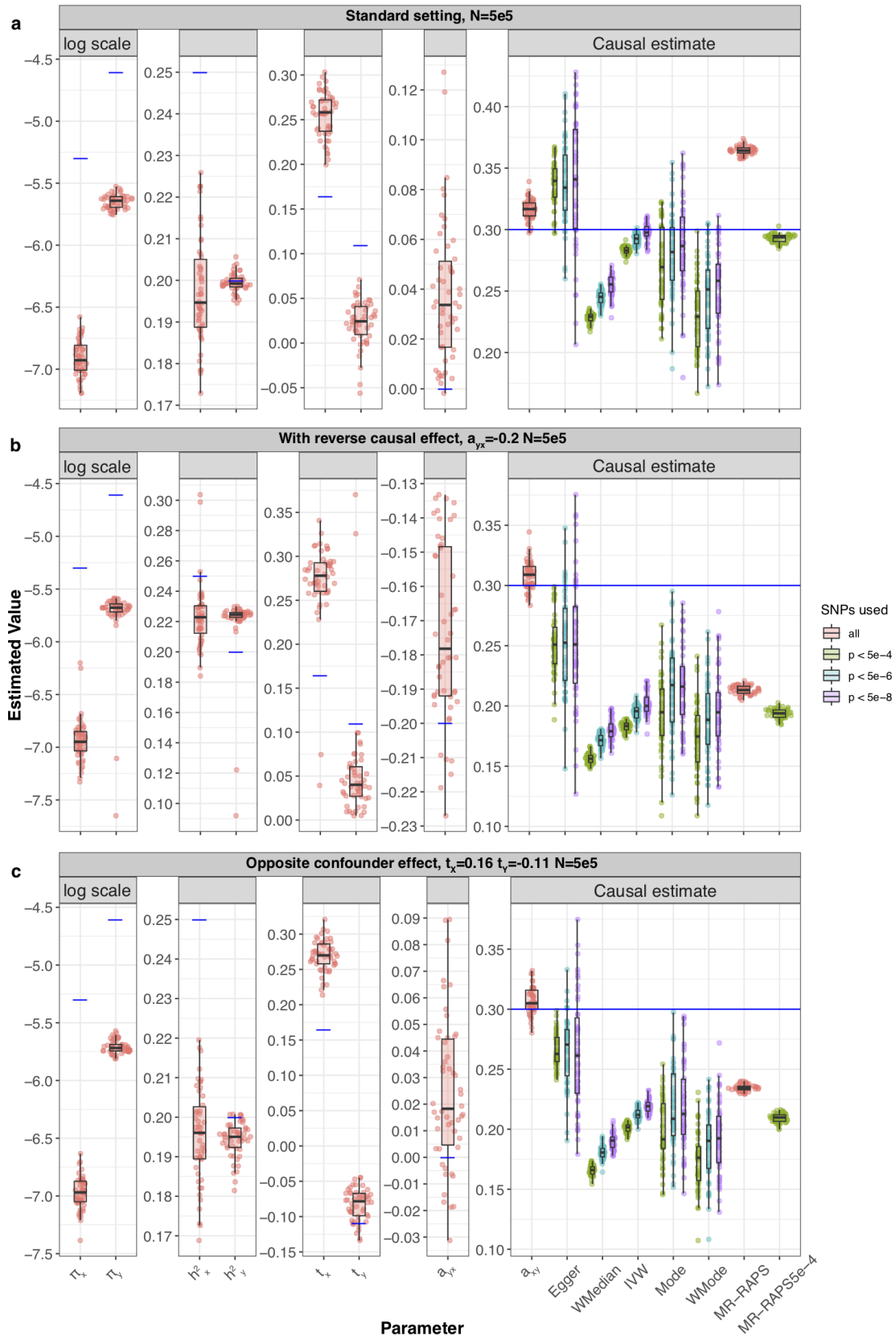
1028 More often than not, only one slope is recovered within the boundaries of the parameters set  
1029 for LHC-MR. However, given the now known re-parameterisation, the second (and if found,  
1030 third) slope can be simply calculated if not found by the likelihood function minimisation. It  
1031 is reasonable to assume that the direct heritability of each trait is larger than the indirect  
1032 heritability, hence we report parameter sets where  $h_x^2 > t_x^2$  or  $h_y^2 > t_y^2$ .



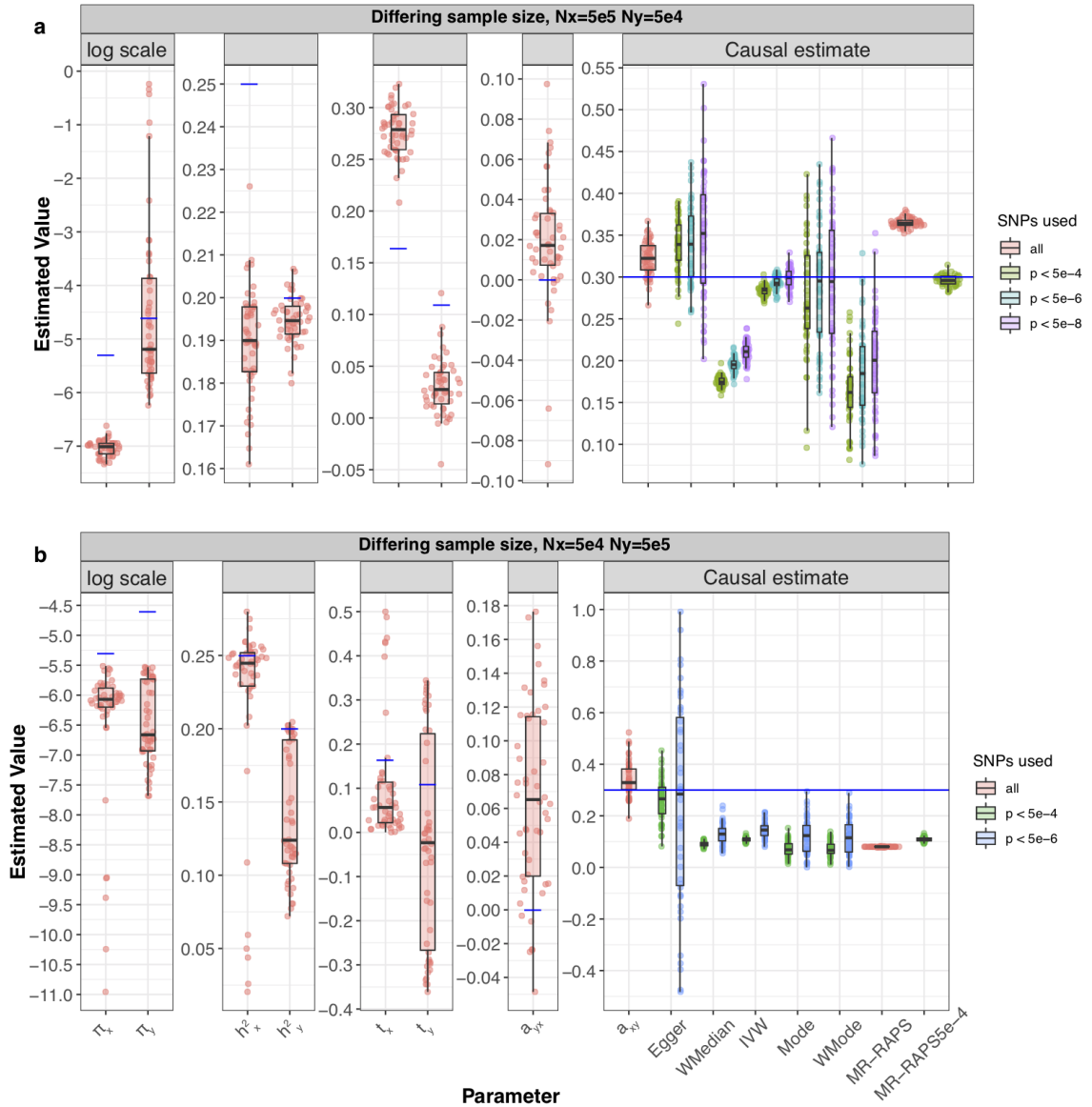
**Figure S2:** An illustration of a scatter plot showing simulated observed SNP effects on traits  $X$  and  $Y$ , coloured by the strongest effect between the three vectors  $\gamma_x, \gamma_y, \gamma_u$ . SNPs in grey are those with no effect on any of the traits. This illustration shows the distinct clusters that could arise in the presence of a confounder. The dark blue cluster of SNPs represents those that are not in violation of any of the MR assumption, and hence its slope reflects the true causal effect of  $X$  on  $Y$ , while the red cluster of SNPs are those associated with the confounder. The steeper slope of the red cluster of SNPs causes a typical regression line - shown in grey - that represents the causal effect (estimated using conventional MR methods) to be overestimated.



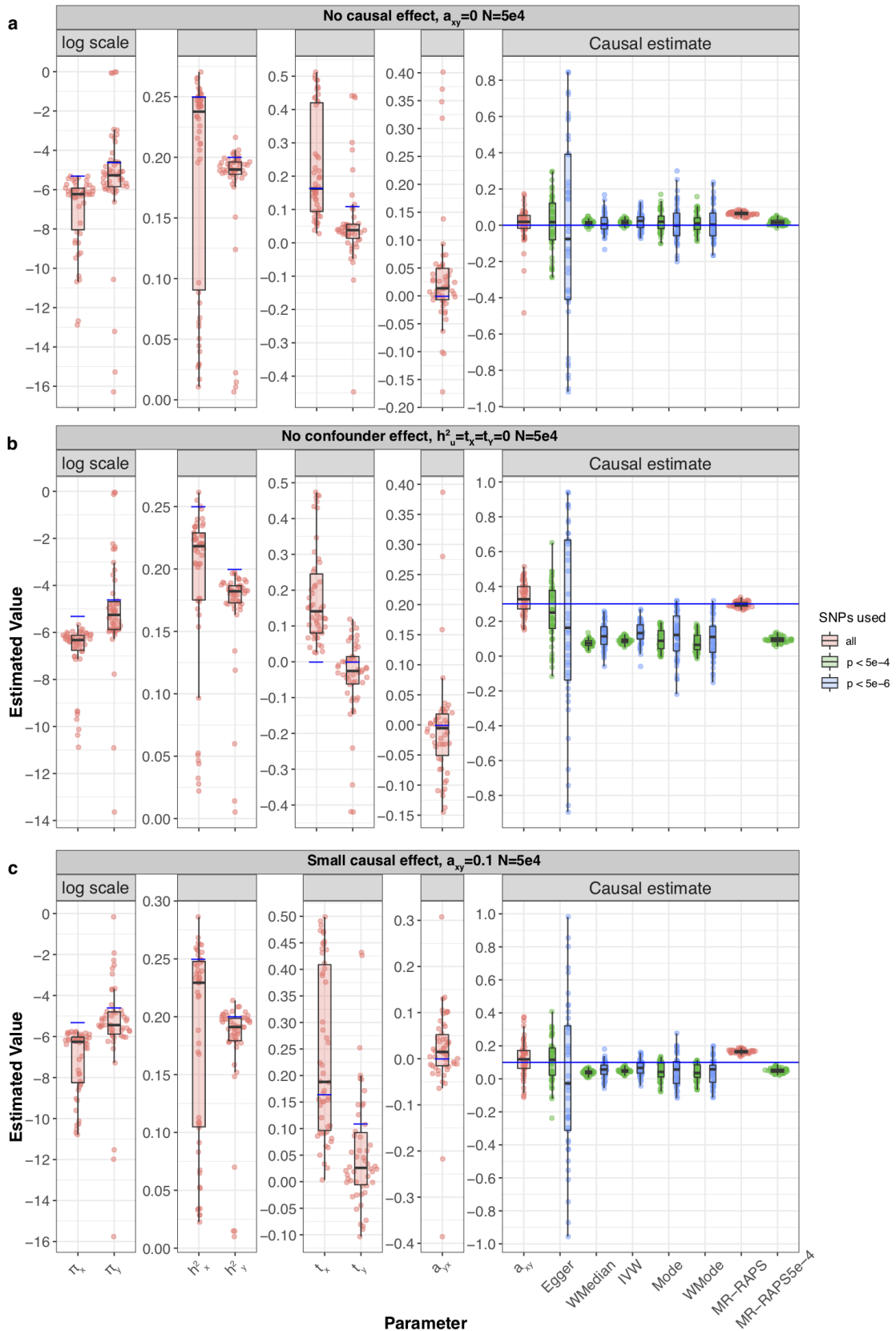
**Figure S3: A schema showing the workflow of the simulation results.** For a single set of parameter settings, 50 different data generations of GWAS summary statistics are created for trait  $X$  and  $Y$ . The summary statistics of a single data generation, as well as the sample size, SNP number and SNP-based LD structure are used in the likelihood optimisation function that is run with 100 different random starting points in order to explore the likelihood surface. A single maximum likelihood and its corresponding estimated parameters are selected to represent the estimates of that data generation. And this is repeated for the other generations. The results for several data generation are often represented in boxplots throughout the paper.



**Figure S4: Simulation results under various scenarios.** These Raincloud boxplots<sup>28</sup> represent the distribution of parameter estimates from 50 different data generations under various conditions. For each generation, standard MR methods as well as our LHC-MR were used to estimate a causal effect. The true values of the parameters used in the data generations are represented by the blue dots/lines. **a** Estimation under standard settings ( $\pi_x = 5 \times 10^{-3}, \pi_y = 1 \times 10^{-2}, \pi_u = 5 \times 10^{-2}, h_x^2 = 0.25, h_y^2 = 0.2, h_u^2 = 0.3, t_x = 0.16, t_y = 0.11$ ). **b** Addition of a reverse causal effect  $\alpha_{y \rightarrow x} = -0.2$ . **c** Confounder with opposite causal effects on  $X$  and  $Y$  ( $t_x = 0.16, t_y = -0.11$ ).

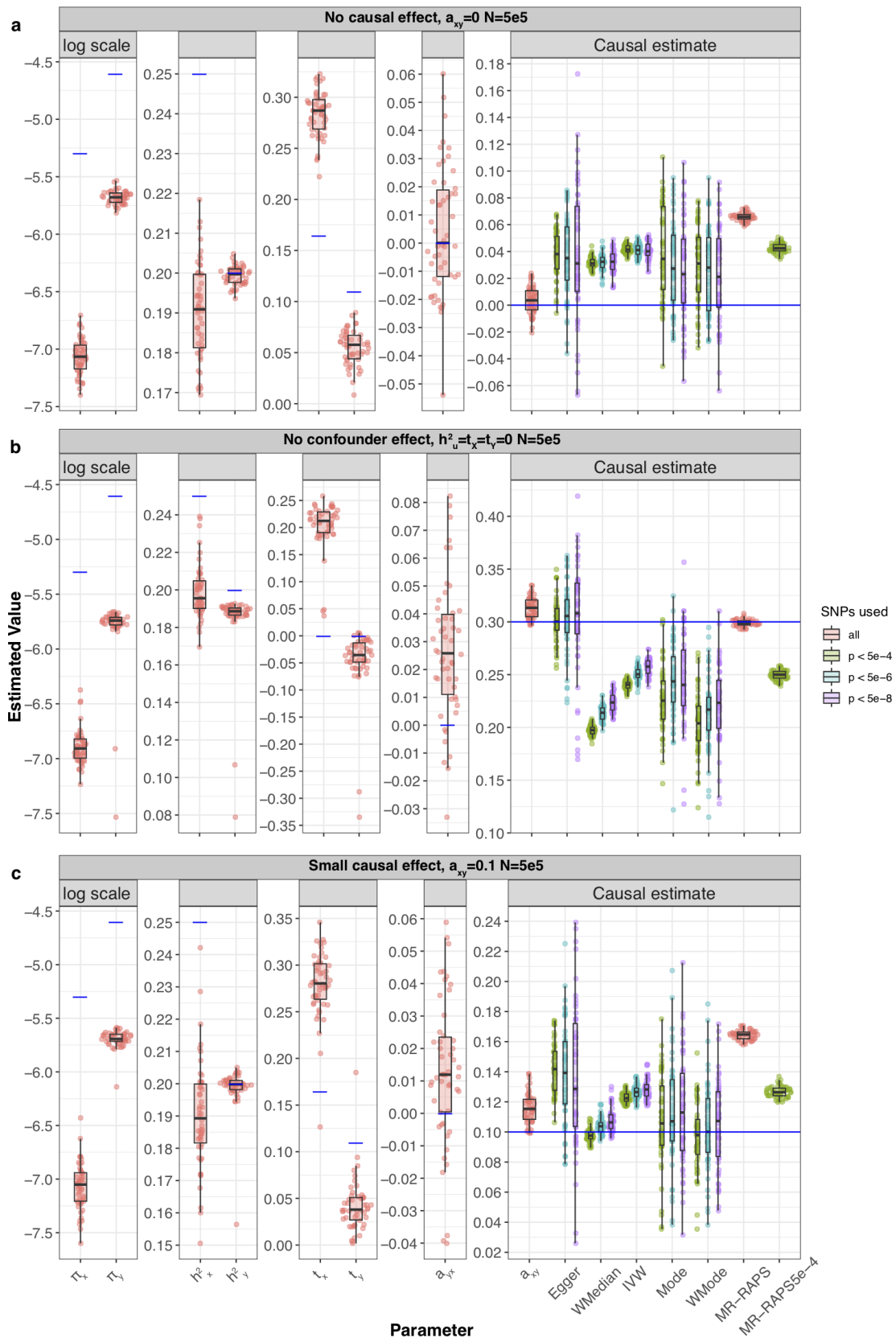


**Figure S5: Simulation results showing varying sample sizes for the two exposure and outcome samples.** Raincloud boxplots representing the distribution of parameter estimates from 50 different data generations. For each generation, standard MR methods as well as our LHC-MR were used to estimate a causal effect. The true values of the parameters used in the data generations are represented by the blue dots/lines. In this figure, samples sizes for the two traits differ as such  $n_x = 500,000$  and  $n_y = 50,000$  for **a**, and  $n_x = 50,000$  and  $n_y = 500,000$  for **b**.

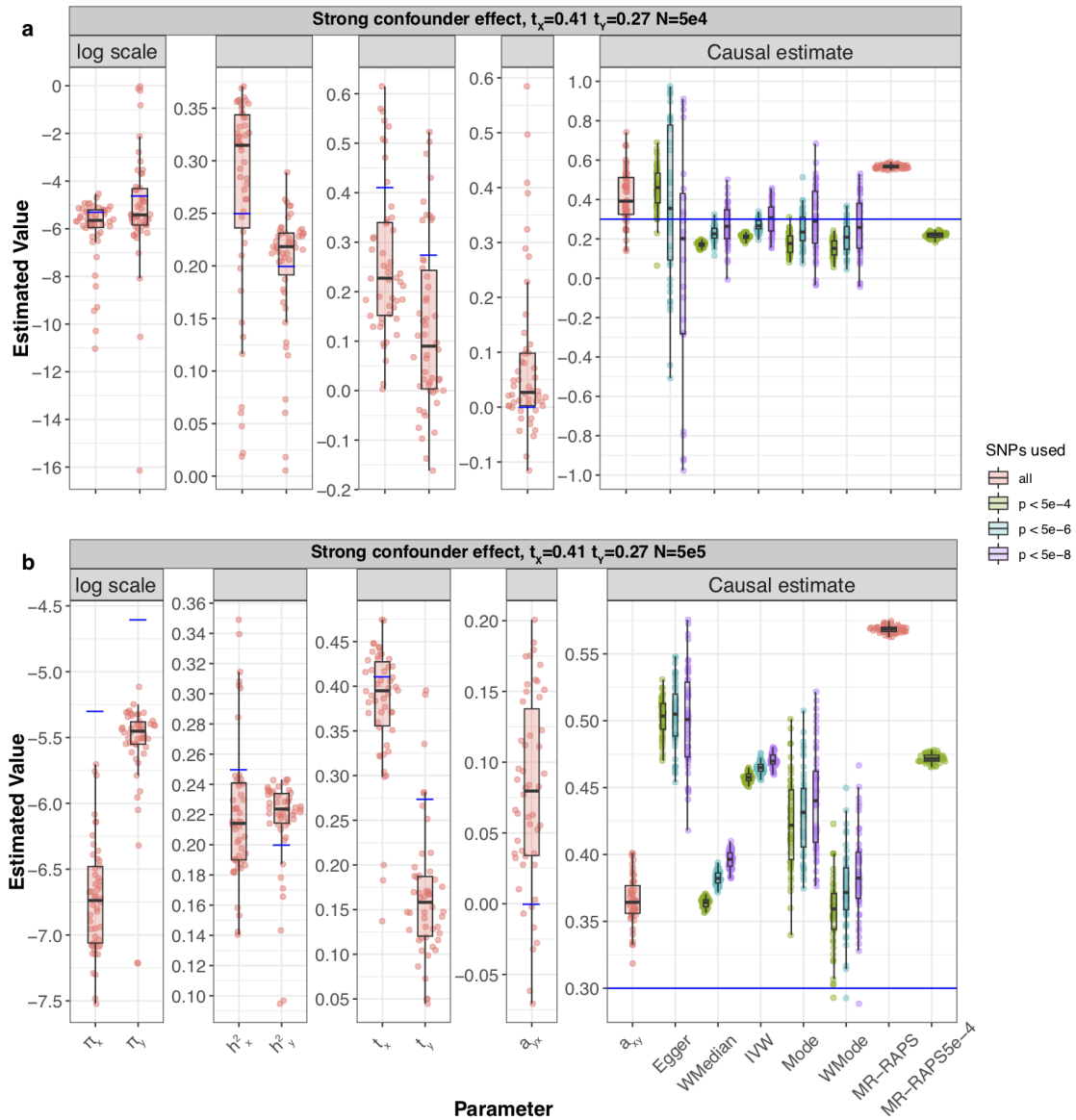


**Figure S6: Simulation results under various scenarios.** These Raincloud boxplots<sup>28</sup> represent the distribution of parameter estimates from 50 different data generations under various conditions. For each generation, standard MR methods as well as our LHC-MR were used to estimate a causal effect. The true values of the parameters used in the data generations are represented by the blue dots/lines. **a** The data simulated had no causal effect in either direction. **b** The data simulated had no confounder effect with  $\pi_u, t_x,$  and  $t_y = 0$ . **c** This model had a small causal effect of  $\alpha_{x \rightarrow y} = 0.1$ .

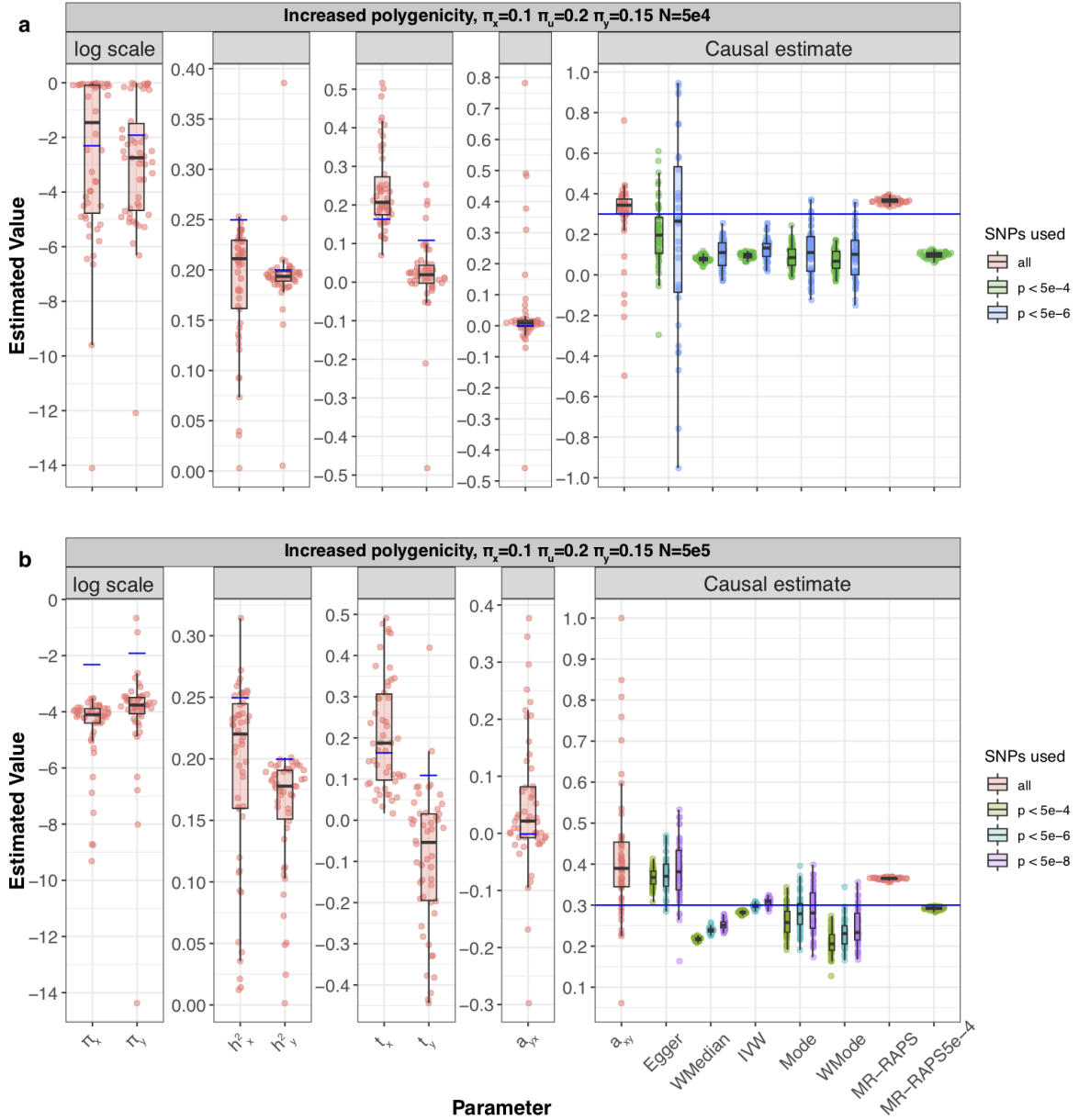




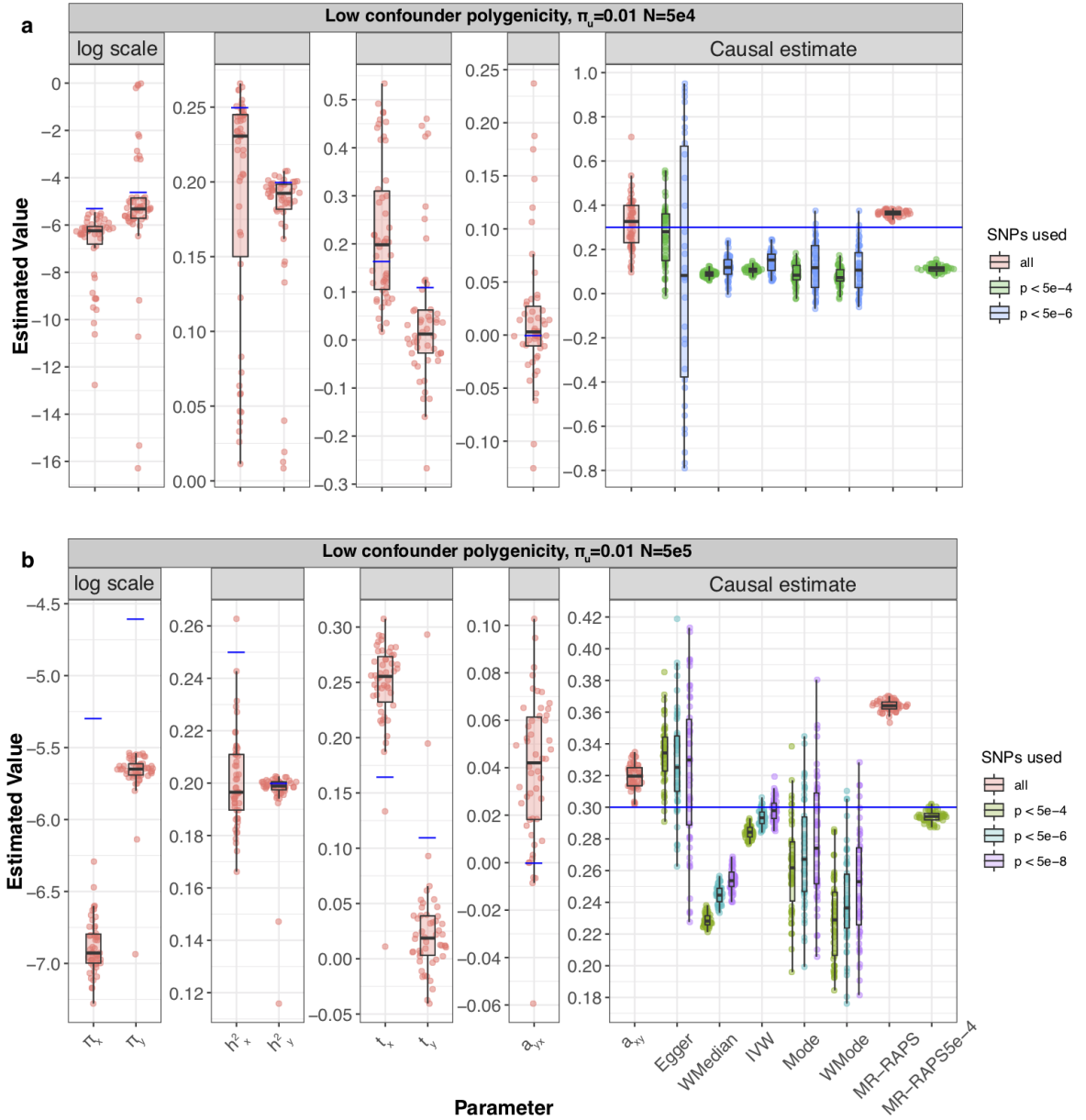
**Figure S7: Simulation results under various scenarios.** These Raincloud boxplots<sup>28</sup> represent the distribution of parameter estimates from 50 different data generations under various conditions. For each generation, standard MR methods as well as our LHC-MR were used to estimate a causal effect. The true values of the parameters used in the data generations are represented by the blue dots/lines. **a** The data simulated had no causal effect in either direction. **b** The data simulated had no confounder effect with  $\pi_u, t_x,$  and  $t_y = 0$ . **c** This model had a small causal effect of  $\alpha_{x \rightarrow y} = 0.1$ .



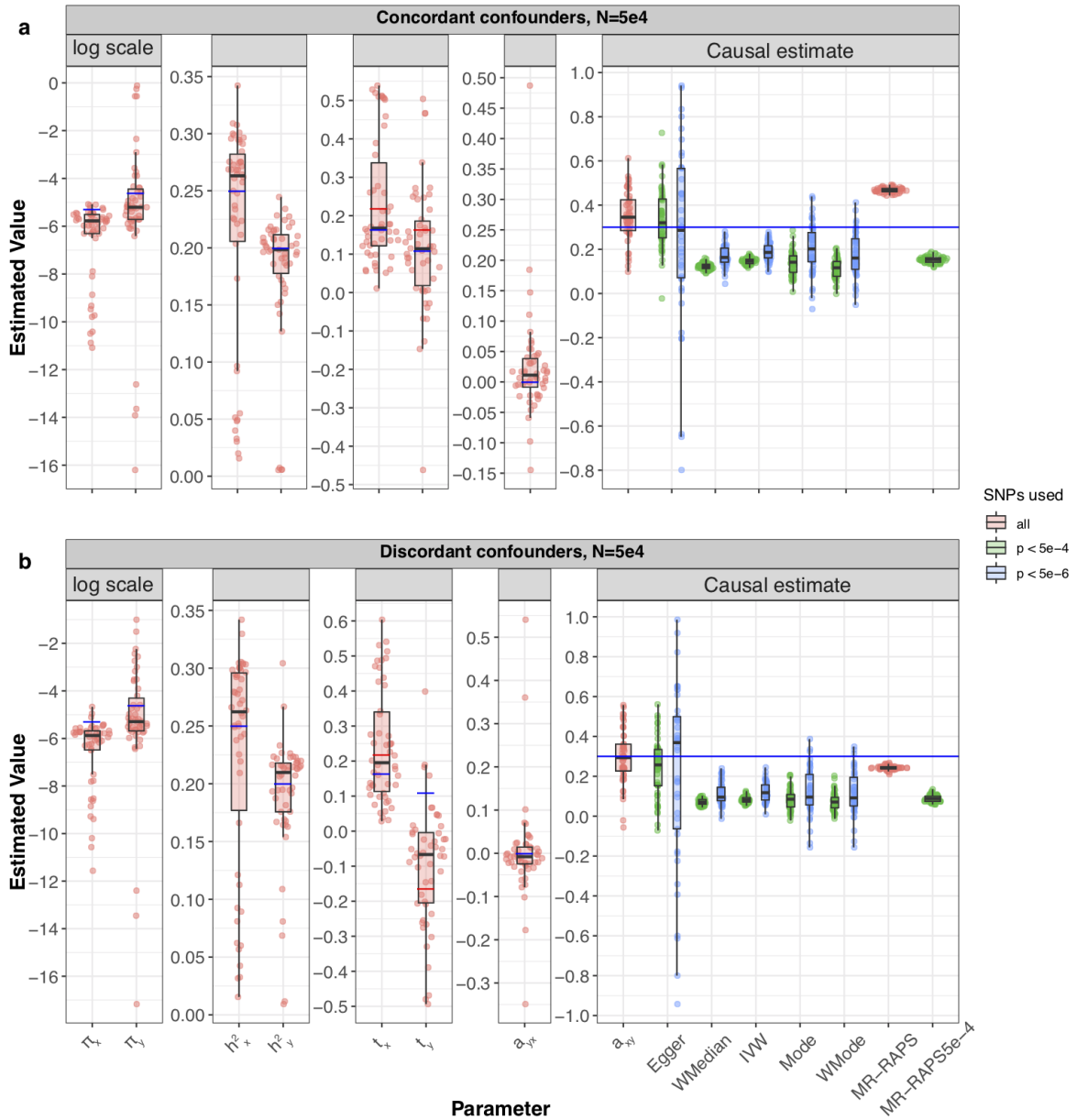
**Figure S8: Simulation results under various scenarios.** These Raincloud boxplots<sup>28</sup> represent the distribution of parameter estimates from 50 different data generations under various conditions. For each generation, standard MR methods as well as our LHC-MR were used to estimate a causal effect. The true values of the parameters used in the data generations are represented by the blue dots/lines. **a** The data simulated shows the increased effect of  $U$  on  $X$  and  $Y$  through  $t_x = 0.41, t_y = 0.27$  instead of the standard setting  $t_x = 0.16, t_y = 0.11$ . **b** This panel show the same thing but with a larger sample size of  $n_x = n_y = 500,000$



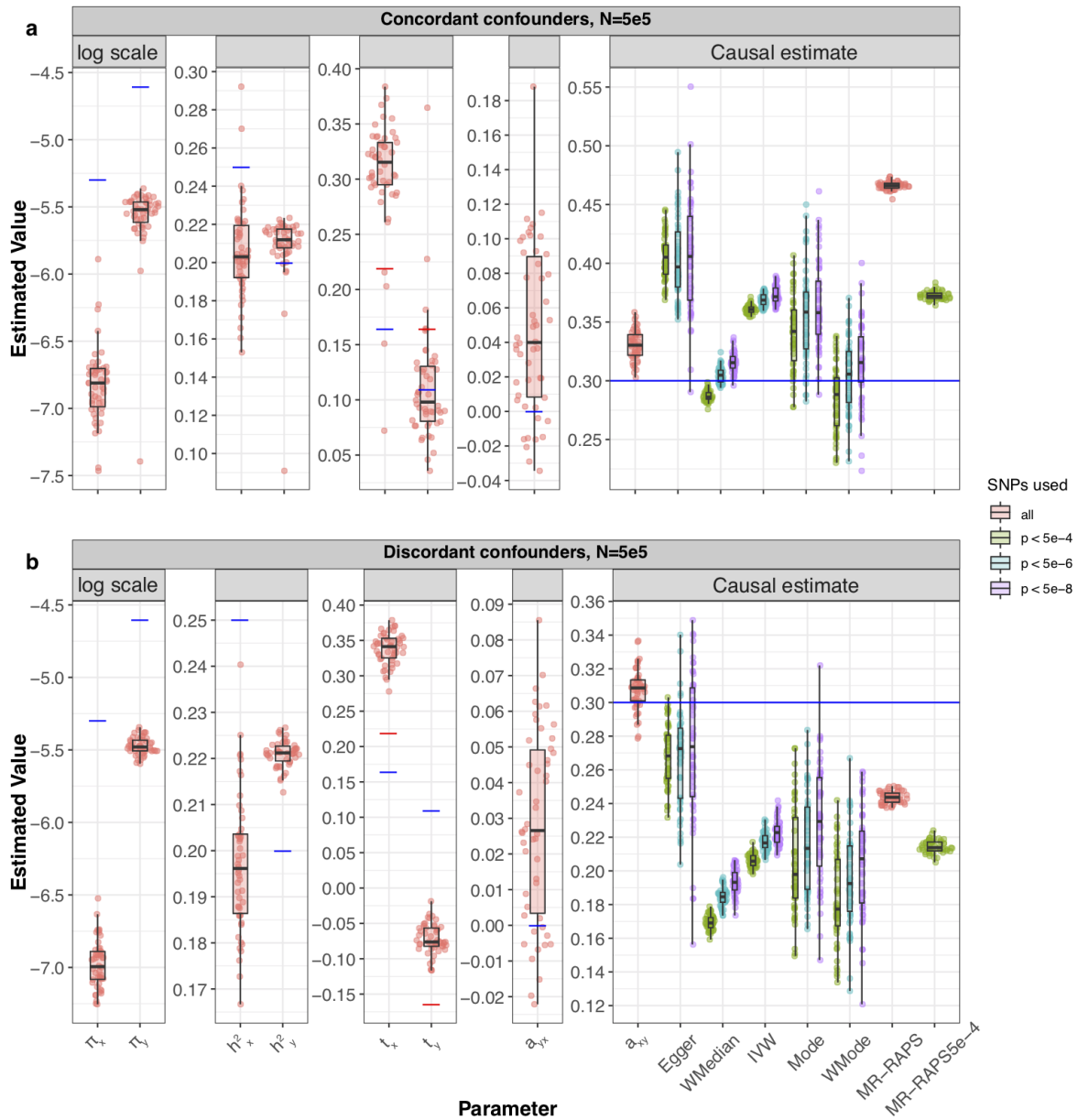
**Figure S9: Simulation results where there is an increased polygenicity for all traits.** Boxplots representing the distribution of parameter estimates from 100 different data generations. For each generation, standard MR methods as well as our LHC-MR were used to estimate a causal effect. The true values of the parameters used in the data generations are represented by the blue dots/lines. The proportion of effective SNPs that make up the spike-and-slab distributions of the  $\gamma$  vectors in this setting is 10%, 15%, and 20% for traits  $X$ ,  $Y$  and  $U$  respectively. **a** Results for smaller sample size of  $n_x = n_y = 50,000$ . **b** Results for larger sample size of  $n_x = n_y = 500,000$ .



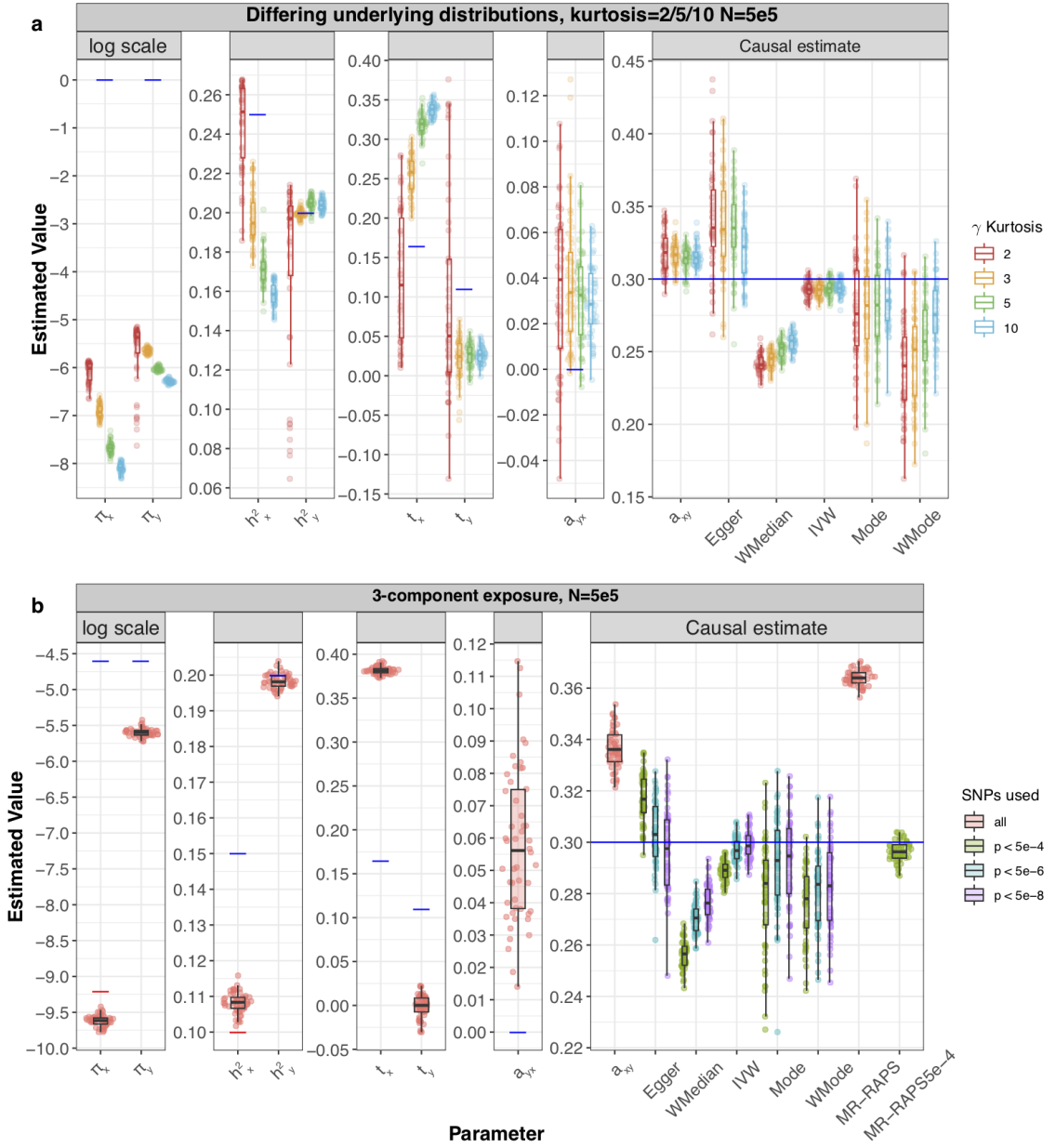
**Figure S10: Simulation results where the polygenicity of the confounder is reduced.** Boxplots representing the distribution of parameter estimates from 100 different data generations. For each generation, standard MR methods as well as our LHC-MR were used to estimate a causal effect. The true values of the parameters used in the data generations are represented by the blue dots/lines. In this figure, the polygenicity for  $U$  is decreased in the form of lower  $\pi_u = 0.01$ . **a** Results for smaller sample size of  $n_x = n_y = 50,000$ . **b** Results for larger sample size of  $n_x = n_y = 500,000$ .



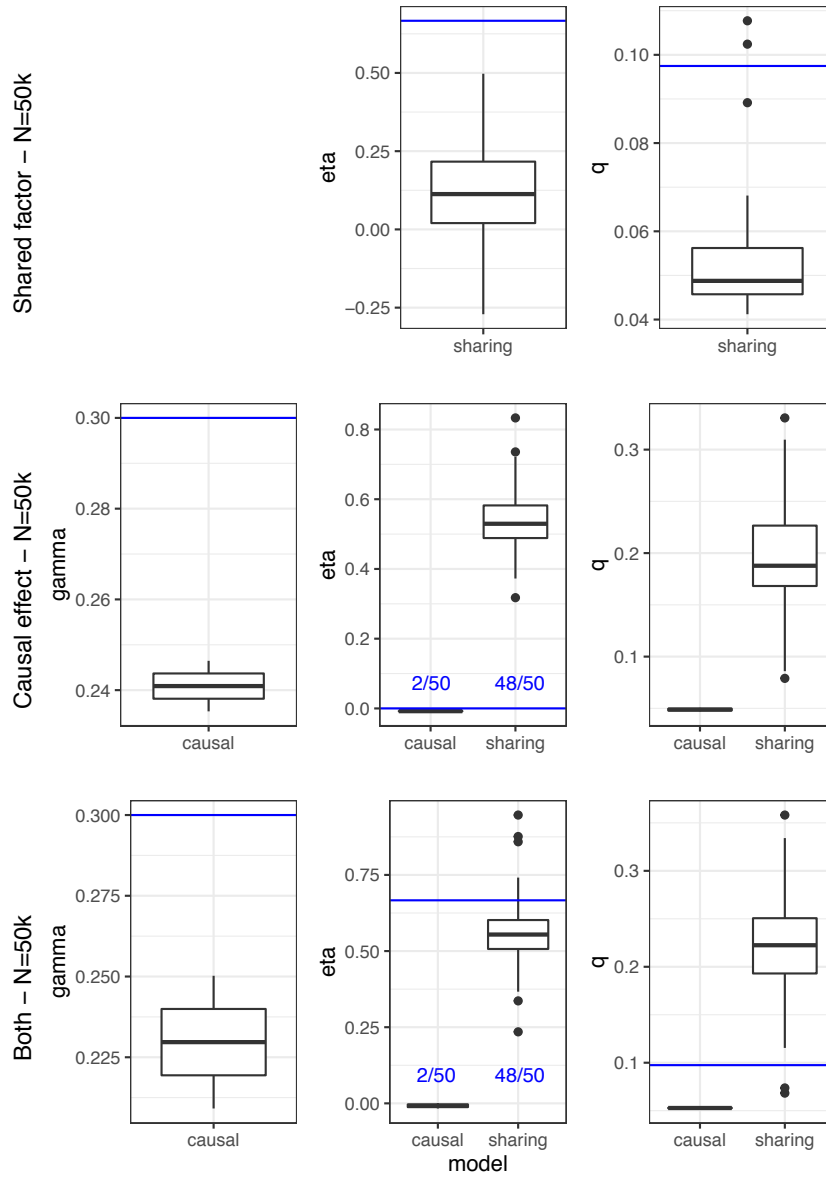
**Figure S11: Simulation results where there are two underlying confounders, once with concordant and another with discordant effects on the exposure-outcome pair.** Boxplots representing the distribution of parameter estimates from 100 different data generations. For each generation, standard MR methods as well as our LHC-MR were used to estimate a causal effect. The true values of the parameters used in the data generations are represented by the blue dots/lines. **a** The underlying data generations have two concordant heritable confounders  $U_1$  and  $U_2$  with positive effects on traits  $X$  and  $Y$ . **b** The data generations have two discordant heritable confounders with  $t_x^{(1)} = 0.16$ ,  $t_y^{(1)} = 0.11$  shown as blue dots and  $t_x^{(2)} = 0.22$ ,  $t_y^{(2)} = -0.16$  shown as red dots.



**Figure S12: Simulation results where there are two underlying confounders, once with concordant and another with discordant effects on the exposure-outcome pair.** Boxplots representing the distribution of parameter estimates from 100 different data generations. For each generation, standard MR methods as well as our LHC-MR were used to estimate a causal effect. The true values of the parameters used in the data generations are represented by the blue dots/lines. **a** The underlying data generations have two concordant heritable confounders  $U_1$  and  $U_2$  with positive effects on traits  $X$  and  $Y$ . **b** The data generations have two discordant heritable confounders with  $t_x^{(1)} = 0.16$ ,  $t_y^{(1)} = 0.11$  shown as blue dots and  $t_x^{(2)} = 0.22$ ,  $t_y^{(2)} = -0.16$  shown as red dots.

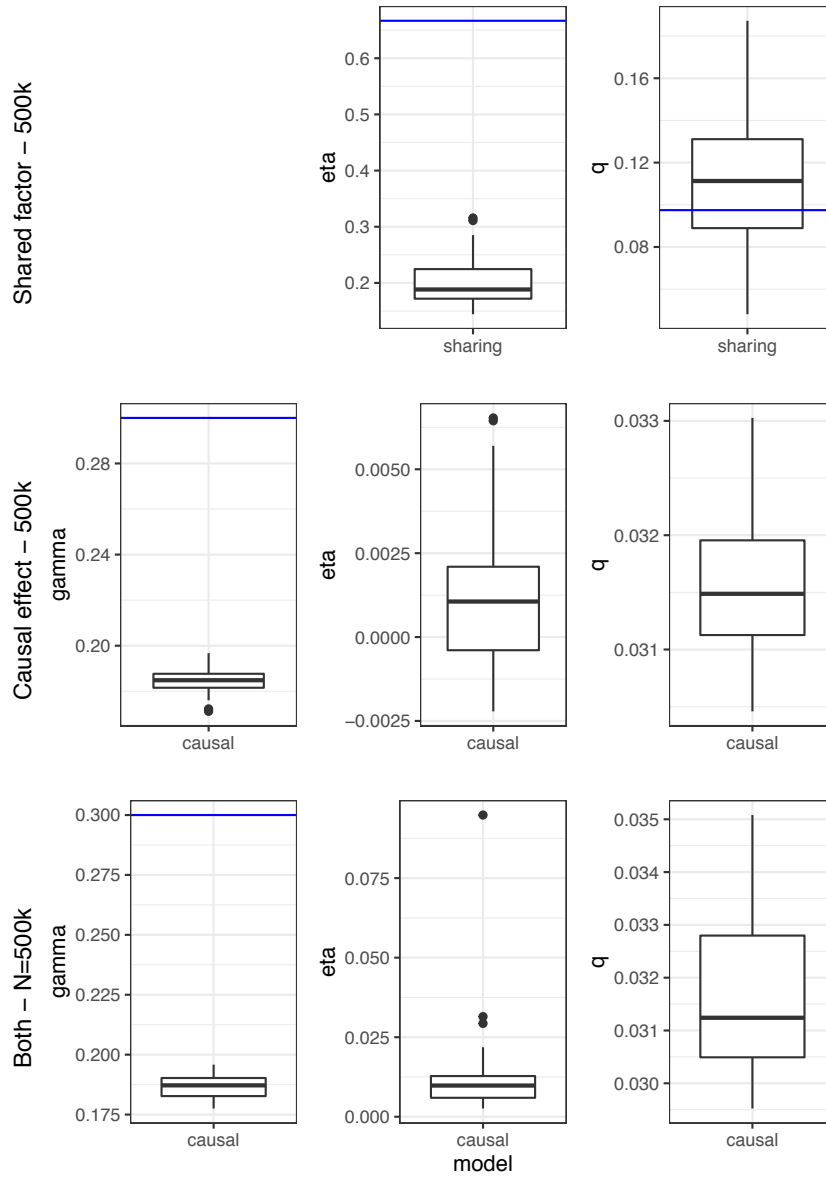


**Figure S13: Simulation results under various scenarios.** These Raincloud boxplots<sup>28</sup> represent the distribution of parameter estimates from 50 different data generations under various conditions. For each generation, standard MR methods as well as our LHC-MR were used to estimate a causal effect. The true values of the parameters used in the data generations are represented by the blue dots/lines. **a** The different coloured boxplots represent the underlying non-normal distribution used in the simulation of the three  $\gamma_x, \gamma_x, \gamma_u$  vectors associated to their respective traits. The Pearson distributions had the same 0 mean and skewness, however their kurtosis ranged between 2 and 10, including the kurtosis of 3, which corresponds to a normal distribution assumed by our model. The standard MR results reported had IVs selected with a p-value threshold of  $5 \times 10^{-6}$ . **b** Addition of a third component for exposure  $X$ , while decreasing the strength of  $U$ . True parameter values are in colour, blue and red for each component ( $\pi_{x1} = 1 \times 10^{-4}, \pi_{x2} = 1 \times 10^{-2}, h_{x1}^2 = 0.15, h_{x2}^2 = 0.1$ ).

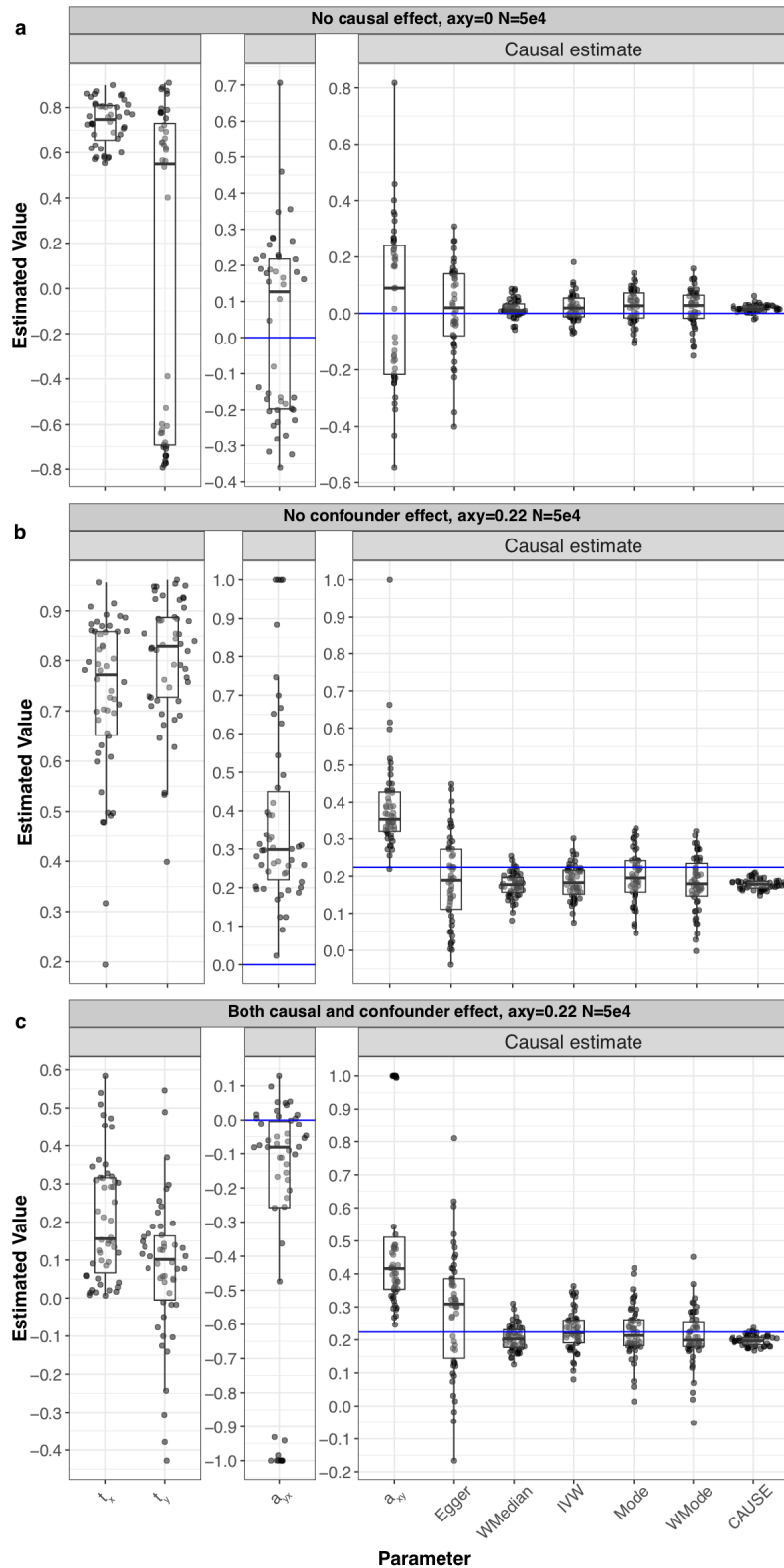


**Figure S14: Running CAUSE on LHC-MR simulated data under the standard settings.** Boxplots of the parameter estimation of CAUSE on LHC-simulated data ( $n_x = n_y = 50,000$ ) under three different scenarios: presence of a shared factor only, presence of a causal effect only, presence of both. CAUSE returns two possible models with a respective p-value, the sharing and the causal model, where the causal mode is the significant of the two. When only an underlying shared factor was present in the simulated data, CAUSE had no significant causal estimates. With a true underlying causal effect, or when both an underlying causal effect and a shared factor was present, the causal model was significant only 4% of the simulations.

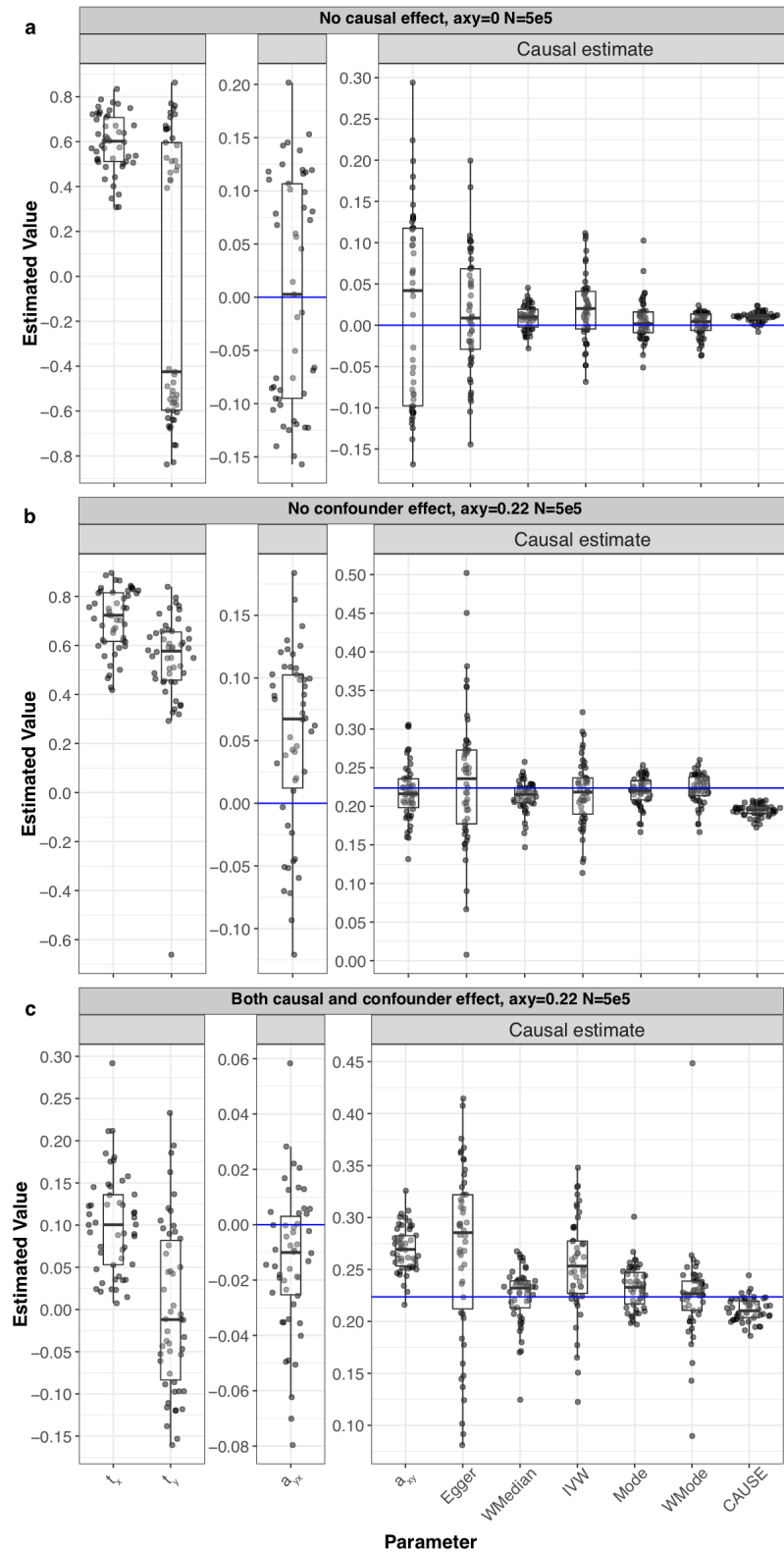




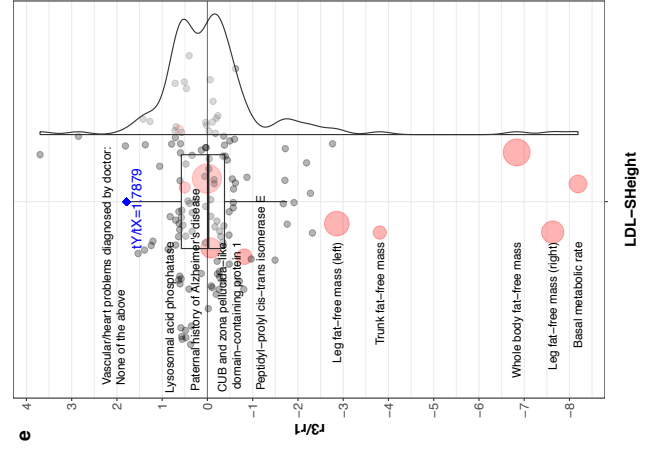
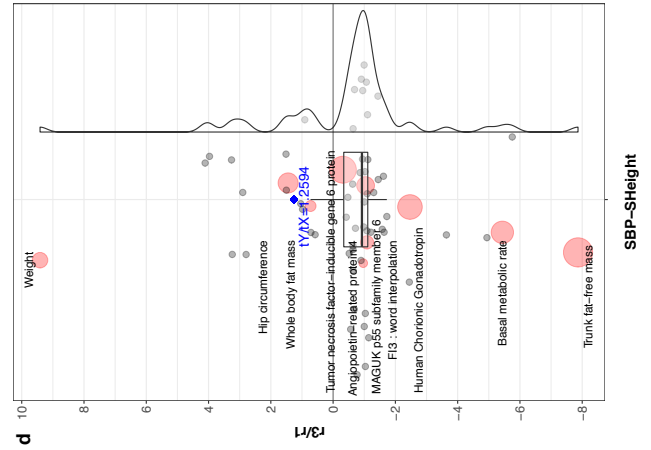
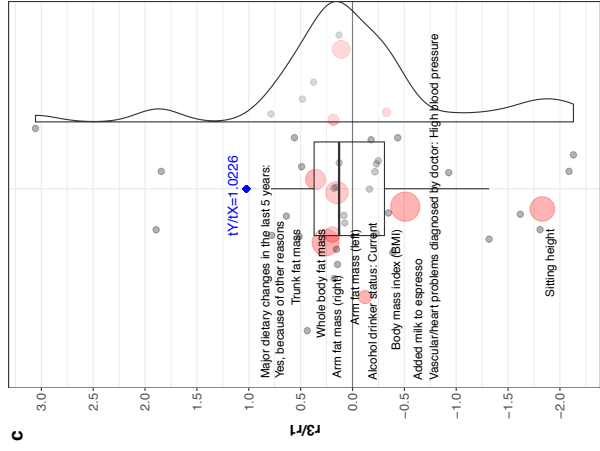
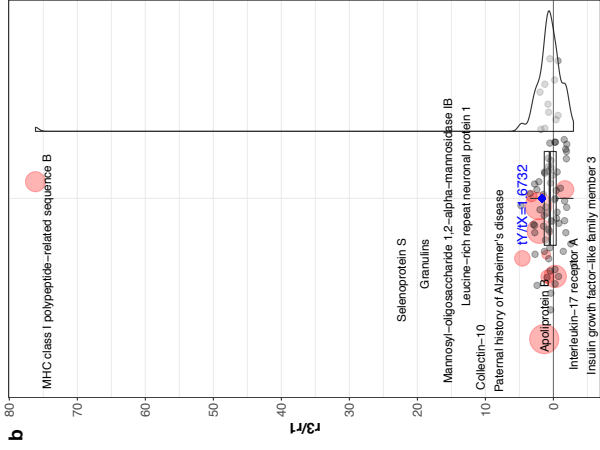
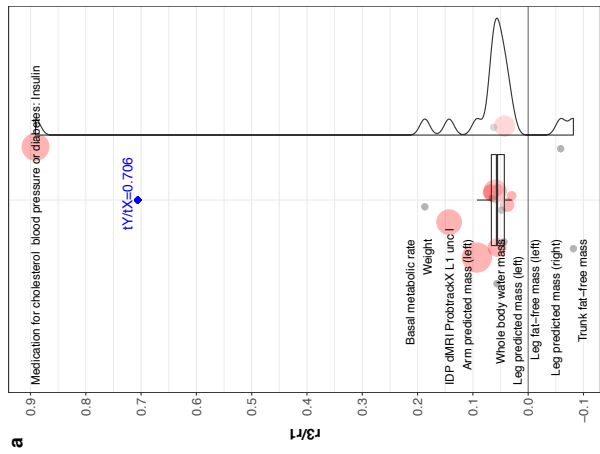
**Figure S15: Running CAUSE on LHC-MR simulated data under the standard settings.** Boxplots of the parameter estimation of CAUSE on LHC-simulated data ( $n_x = n_y = 500,000$ ) under three different scenarios: presence of a shared factor only, presence of a causal effect only, presence of both. CAUSE returns two possible models with a respective p-value, the sharing and the causal model, where the causal mode is the significant of the two. When only an underlying shared factor was present in the simulated data, CAUSE had no significant causal estimates. With a true underlying causal effect, or when both an underlying causal effect and a shared factor was present, the causal model was significant 100% of the simulations.



**Figure S16: Running LHC-MR on CAUSE simulated data under various scenarios.** Rain-cloud boxplots representing the distribution of parameter estimates from LHC-MR of 50 different data generations using the CAUSE framework. For each generation, standard MR methods, CAUSE as well as our LHC-MR were used to estimate a causal effect. The true values of the parameters used in the data generations are represented by the blue dots/lines. **a** CAUSE data was generated with no causal effect but with a shared factor with an  $\eta$  value of  $\sim 0.22$ . CAUSE chooses a sharing model 100% of the time with no estimate for a causal effect. **b** CAUSE is simulated with causal effect but with no shared factor. **c** CAUSE is simulated with both a causal effect and a shared factor.



**Figure S17: Running LHC-MR on CAUSE simulated data under various scenarios.** Rain-cloud boxplots representing the distribution of parameter estimates from LHC-MR of 50 different data generations using the CAUSE framework. For each generation, standard MR methods, CAUSE as well as our LHC-MR were used to estimate a causal effect. The true values of the parameters used in the data generations are represented by the blue dots/lines. **a** CAUSE data was generated with no causal effect but with a shared factor with an  $\eta$  value of  $\sim 0.22$ . **b** CAUSE is simulated with causal effect but with no shared factor. **c** CAUSE is simulated with both a causal effect and a shared factor. LHC-MR seems to exhibit a bimodal effect at first glance, but the two peaks are not connected.



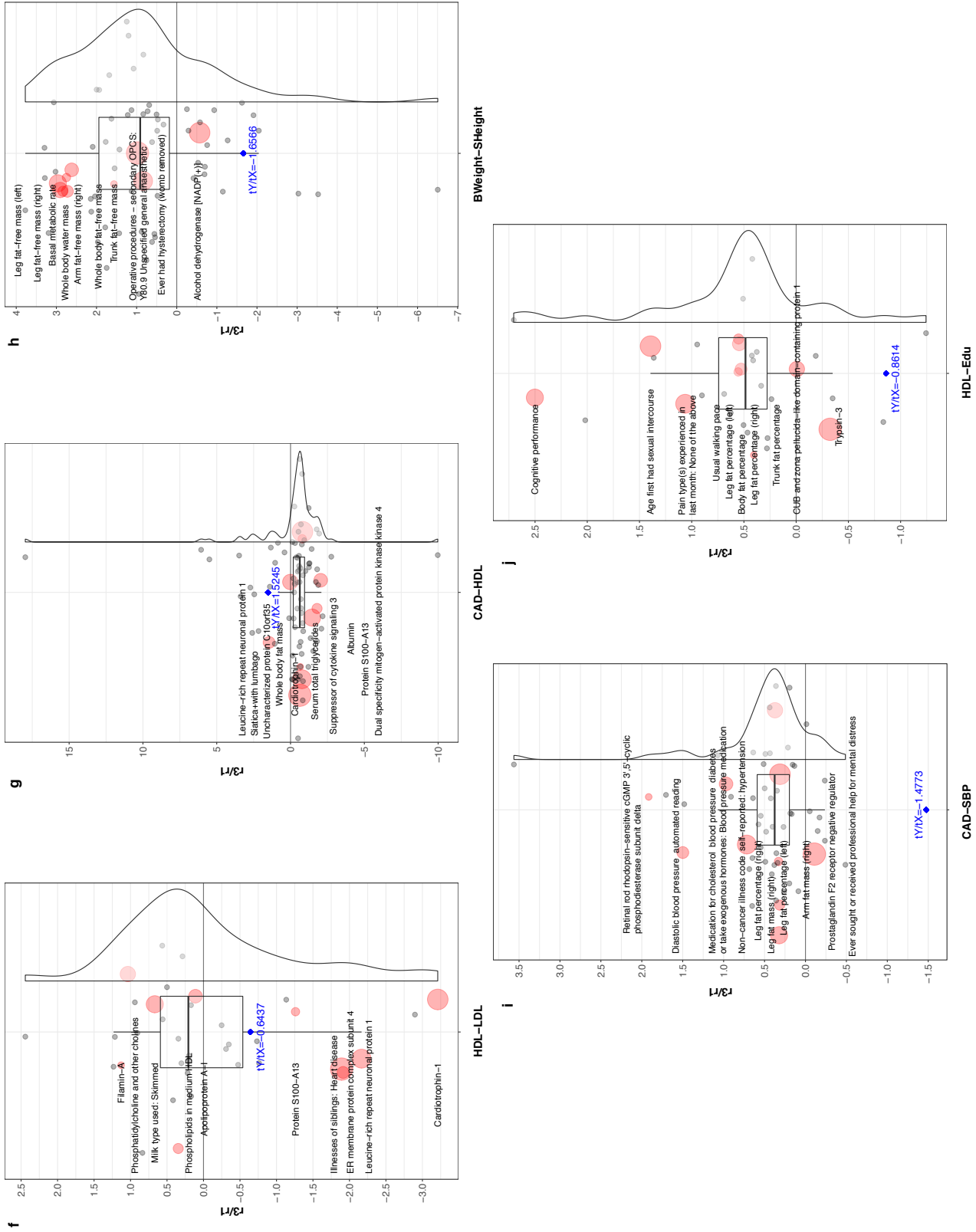


**Figure S18: Confounder effects obtained from EpiGraphDB plotted as a raincloud with the  $r_3/r_1$  ratio on the y-axis.** The blue diamonds represent the  $t_y/t_x$  ratio derived from the LHC model for that trait pair, also reported in blue text. Labelled dots in red and their varying size show the ten largest confounder traits in terms of their absolute effect product on the two traits, whereas grey dots represent the rest of the confounder traits found by EpiGraphDB.

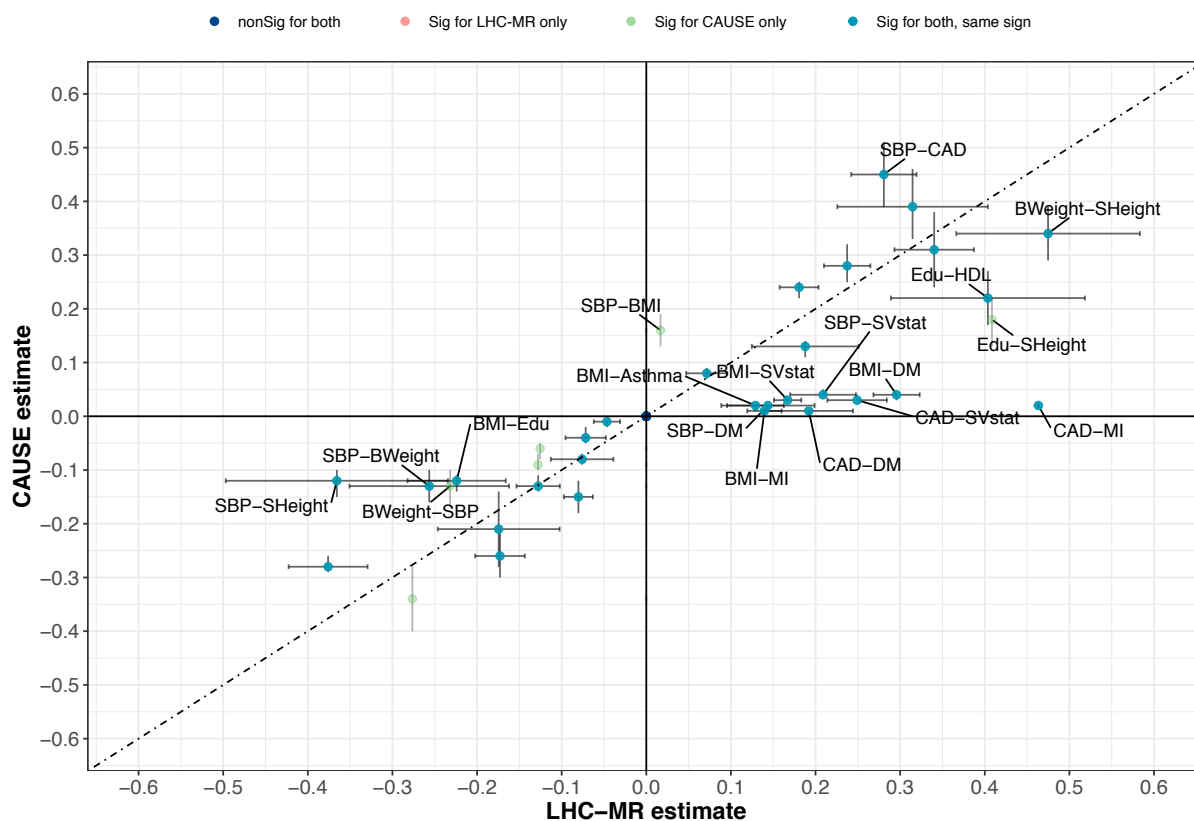


**Figure S19: A scatter plot of the causal effect estimates between LHC-MR and CAUSE.** To improve visibility, non-significant estimates by both methods are placed at the origin, while significant estimates by both methods appear on the diagonal with 95% CI error bars for LHC-MR estimates, and 95% credible interval error bars for CAUSE estimates. Labeled pairs are those with an estimate difference greater than 0.1.

UKBB ID / Data Origin	Trait Name	Abbreviation	Sample Size	PMID
845	Age completed full time education	Edu	240,547	25826379
21001_irnt	Body mass index (BMI)	BMI	359,983	25826379
2443	Diabetes diagnosed by doctor	DM	360,192	25826379
20002_1075	Non-cancer illness code, self-reported: heart attack/myocardial infarction	MI	361,141	25826379
20002_1111	Non-cancer illness code, self-reported: asthma	Asthma	361,141	25826379
2887	Number of cigarettes previously smoked daily	PSmoke	84,456	25826379
20022_irnt	Birth weight	BWeight	205,475	25826379
50_irnt	Standing height	SHeight	360,388	25826379
4080	Systolic blood pressure, automated reading	SBP	340,159	25826379
20003_1140861958	Treatment/medication code: simvastatin	SVstat	361,141	25826379
30780_irnt	LDL Cholesterol	LDL	343,621	25826379
30760_irnt	HDL Cholesterol	HDL	315,133	25826379
UKBB + CARDIoGRAMplusC4D	Coronary Artery Disease	CAD	380,831	29212778

**Table S1:** Details of the origin study of each trait, its abbreviation used in this paper, the sample size of the study for that trait, as well as the PubMed article ID.

a		MR-Egger			b		WMedian			c		IVW		
LHC-MR		Sig+	Sig-	nonSig		Sig+	Sig-	nonSig		Sig+	Sig-	nonSig		
	Sig+	10	0	27	Sig+	21	1	15	Sig+	23	0	14		
	Sig-	0	2	35	Sig-	0	12	25	Sig-	0	17	20		
	nonSig	0	2	56	nonSig	1	6	51	nonSig	2	5	51		

d		Mode			e		WMode			f		WMode		
LHC-MR		Sig+	Sig-	nonSig		Sig+	Sig-	nonSig	MR-Egger		Sig+	Sig-	nonSig	
	Sig+	12	0	25	Sig+	13	3	21		Sig+	10	0	0	
	Sig-	0	2	35	Sig-	0	7	30		Sig-	0	1	3	
	nonSig	0	0	58	nonSig	0	2	56		nonSig	3	11	104	

**Table S7:** Cross tables between LHC-MR and various standard MR methods comparing the significance and sign of each respective causal estimate. **f** shows a cross table between the two-least correlated MR methods in terms of their estimates.



Pair	$\alpha_{x \rightarrow y}$	p-value	$\gamma$	IVW $\alpha_{x \rightarrow y}$	p-value
BMI-Asthma	0.1290	4.99E-14	0.02 (0.01, 0.02)	0.0593	1.00E-08
BMI-DM	0.2958	1.07E-99	0.04 (0.03, 0.04)	0.2447	2.25E-140
BMI-SBP	0.1878	5.55E-09	0.13 (0.11, 0.14)	0.1547	1.11E-24
BMI-SVstat	0.1670	2.08E-91	0.03 (0.03, 0.03)	0.1570	4.26E-63
BMI-MI	0.1396	1.67E-41	0.01 (0.01, 0.01)	0.1027	9.16E-32
BWeight-SHeight	0.4748	9.60E-18	0.34 (0.29, 0.39)	0.2959	8.01E-10
SHeight-BWeight	0.1806	1.93E-53	0.24 (0.22, 0.25)	0.1803	7.21E-86
SBP-DM	0.1437	3.17E-07	0.02 (0.01, 0.02)	0.0697	3.69E-07
DM-SVstat	0.3147	4.11E-12	0.39 (0.33, 0.46)	0.2524	1.28E-16
SHeight-Edu	0.0715	8.42E-09	0.08 (0.07, 0.09)	0.0643	2.28E-21
SBP-SVstat	0.2089	4.84E-26	0.04 (0.04, 0.05)	0.1853	1.46E-52
Edu-HDL	0.4037	5.25E-12	0.22 (0.17, 0.27)	0.2848	4.06E-08
BMI-CAD	0.2373	2.37E-64	0.28 (0.25, 0.32)	0.1800	2.42E-53
CAD-DM	0.1920	5.92E-13	0.01 (0.01, 0.01)	0.0659	0.002455431
DM-CAD	0.4283	5.60E-19	1.95 (1.26, 2.64)	0.1796	4.15E-05
SBP-CAD	0.2807	2.86E-46	0.45 (0.39, 0.51)	0.2500	9.77E-24
CAD-SVstat	0.2491	8.82E-44	0.03 (0.03, 0.04)	0.3077	1.15E-25
CAD-MI	0.4634	0	0.02 (0.02, 0.02)	0.4191	3.07E-285
LDL-CAD	0.3402	1.17E-45	0.31 (0.24, 0.38)	0.2014	8.56E-27
BMI-Edu	-0.2241	3.74E-14	-0.12 (-0.14, -0.11)	-0.1892	6.15E-35
SHeight-BMI	-0.1278	1.40E-22	-0.13 (-0.14, -0.11)	-0.0854	9.01E-23
SBP-BWeight	-0.2565	9.85E-08	-0.13 (-0.16, -0.1)	-0.1646	1.20E-11
SBP-SHeight	-0.3657	4.81E-08	-0.12 (-0.15, -0.1)	-0.0967	0.004422636
SHeight-SBP	-0.0759	5.74E-05	-0.08 (-0.09, -0.07)	-0.0652	1.25E-15
SHeight-SVstat	-0.0465	4.76E-09	-0.01 (-0.02, -0.01)	-0.0328	6.78E-12
BMI-HDL	-0.3760	3.54E-56	-0.28 (-0.29, -0.26)	-0.3630	3.17E-111
SHeight-LDL	-0.0716	4.26E-09	-0.04 (-0.05, -0.02)	-0.0298	5.07E-06
BWeight-CAD	-0.1745	2.05E-06	-0.21 (-0.28, -0.14)	-0.0978	2.83E-05
SHeight-CAD	-0.0802	3.72E-20	-0.15 (-0.18, -0.12)	-0.0482	2.18E-12
HDL-CAD	-0.1729	7.00E-31	-0.26 (-0.3, -0.21)	-0.0778	5.45E-10

**Table S8:** Table comparing the causal estimates of LHC-MR, CAUSE, and IVW for trait pairs that had a significant causal effect in LHC-MR and CAUSE. The column showing the gamma (causal effect) estimate of the CAUSE method also reports its 95% credible intervals. A complete table for all the studied pairs is found in the Supplementary Table S5.